SURE 静岡大学学術リポジトリ
Shizuoka University REpository

Oriented Crystallization of Polly (ethylene terephthalate) . (A survey of polymer crystallization by X-ray diffraction . chapter 4)

メタデータ	言語: English 出版者: SKP 公開日: 2008-01-31 キーワード (Ja): キーワード (En): 作成者: Asano, Tsutomu, Mina, Md. Forhad メールアドレス: 所属:
URL	http://hdl.handle.net/10297/551

Chapter 4. Oriented Crystallization of Poly (ethylene terephthalate)

4.1 Introduction

Poly (ethylene terephthalate) (PET) has a benzene ring in the monomer unit. As shown in Table 1.2, the monomer length is 10.75 Å in the triclinic crystal. It is well known that PET solidifies into a glassy amorphous substance by quenching from the melt state. Cold drawing of amorphous PET produces a highly oriented state with little crystalline structure. A glass transition temperature of PET is 68-69°C. However, initial crystallization of the drawn PET starts lower than this temperature [1,2]. The crystallinity of the samples gradually increases upon the annealing. Therefore, structural development on the cold drawn PET is quite interesting for understanding the crystallization mechanism of polymers.

The morphology of PET was investigated by several authors. Drawing PET above the glass transition temperature, Bonart found an intermediate paracrystalline structure [3]. The final triclinic structure is achieved from a completely amorphous to a nematic first and then to a smectic state. Yeh and Geil pointed out that glassy PET is primarily composed of ball-like structures in which molecules are in the paracrystalline order, and that strain induced crystallization is caused by rotation, alignment, and perfection of the internal order of the ball-like structures [4,5].

In WAXS patterns of the oriented PET, some reflections are often located up and down from normal layer line positions. This fact indicates that crystals are tilted in the same direction with respect to the unit cell. Thus, a definite crystallographic axis, which deviates from the crystalline c-axis, is parallel to the draw direction. This type of orientation is known as a 'tilted orientation' and was first studied by Daubeny *et al.* [6]. They reported that the crystals, drawn at 75°C and annealed at 210°C, are tilted by 5° in such a way that the $(\bar{2}30)$ plane remains vertical. As a result of the tilted orientation, the $\bar{2}30$ reciprocal lattice is perpendicular to the draw direction. The result is explained by an inclined layer structure, where molecular axes show alternating tilts in the crystalline and amorphous layers [7].

Morphological studies were also performed by Zachmann et al. on the primary crystallization of PET [8-11]. However, the precise mechanism, from an amorphous state to a final triclinic structure through paracrystalline structures, is still under discussions. We have thoroughly investigated the crystallization of drawn PET by WAXS, MAXS and SAXS methods, and the analyzed structure is confirmed by the simulation using the light scattering method. The results were published in a series of articles [1,2,12-14]. In this chapter, we will describe structural developments of drawn PET on the basis of these works.

4.2 Sample Preparation and Characterization

At room temperature (20°C), the glassy PET samples were drawn through a necking stage. Appearance of the cold drawn sample is changed with a drawing speed. For instance, the sample remained transparent while drawing at low speed (~0.1mm/sec), whereas it

became white or opaque at high speed (~10.0mm/sec). In the following discussion, we limit the case at 0.1mm/sec. For the systematic observation, the sample was crystallized at different annealing temperatures (T_a) and times (t_a). The drawn samples, kept in a taut state to maintain their length constant, were annealed in a silicon oil bath or an oven (heated by a hot air). Due to the low heat capacity of the air, t_a was chosen 10^4 sec for the air oven [2].

As main observations, WAXS, MAXS and SAXS of the annealed sample were surveyed. The density of the sample was measured in order to estimate its crystallinity. For confirmation, layer models were illustrated by a computer. These patterns were then photographed on 35mm films, which serve as gratings for the light scattering measurements [12].

4.3 WAXS Measurements

4.3.1 Initial crystallization of the cold drawn PET

The WAXS patterns of the cold-drawn PET annealed in the temperature range of 50-100 °C (t_a =10 s) are presented in Fig.4.1 [2]. X-ray diffraction of the cold drawn sample has a broad maximum on the equator. The pattern does not change upon annealing up to 50°C (Fig.4.1a). Diffuse layer lines, perpendicular to the meridian, indicate the scattering by the oriented molecule, as mentioned in Fig.2.4(ii) (pp14).

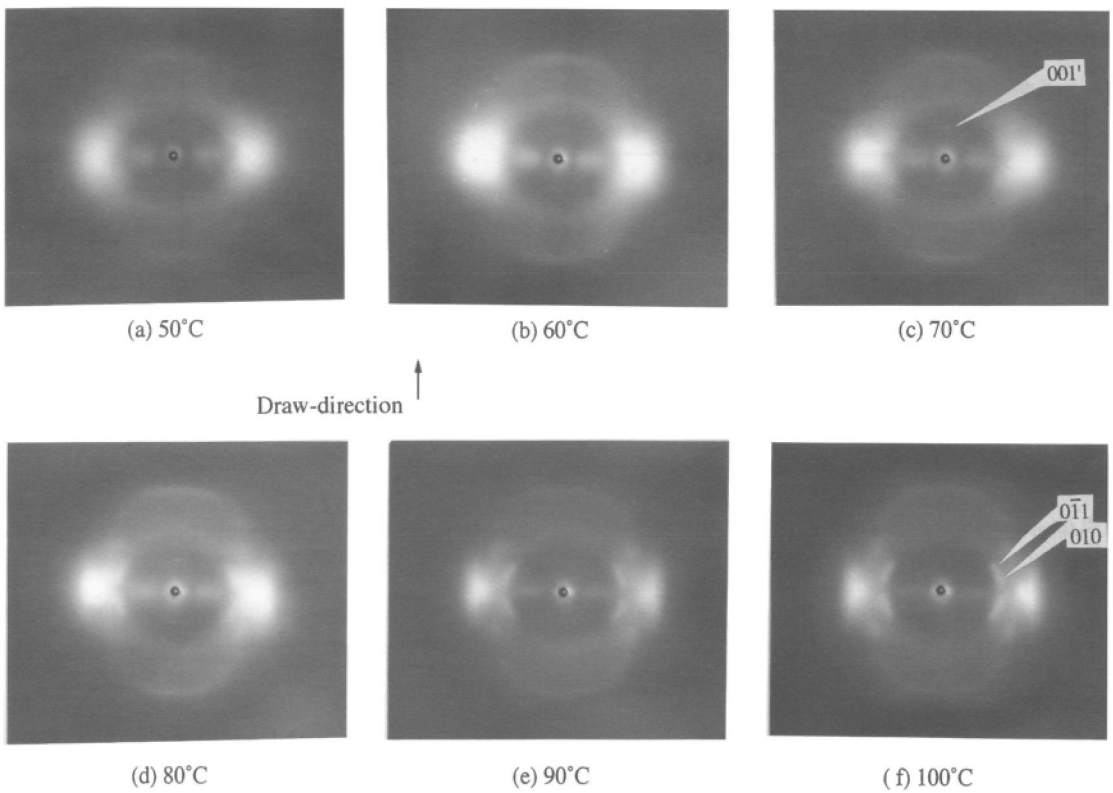

Fig. 4.1 WAXS patterns of PET obtained at different annealing temperatures: (a) 50°C, (b) 60°C, (c) 70°C, (d) 80°C, (e) 90°C, (f) 100°C [2].

The occurrence of a diffuse equatorial maximum indicates that PET molecules are preferentially aligned parallel to the draw direction with absence of a crystalline order, corresponding to a nematic state, which is well known in the liquid crystalline materials.

In Fig.4.1 b–d, a weak reflection appears on the meridian. The spacing of this reflection is measured as 10.7Å. We index this reflection as 001', because the spacing nearly corresponds to the monomer length of PET. The 001' reflection also appears at T_a = 50°C when $t_a = 10^2$s. The equatorial maximum is still broad below 70°C, indicating that the oriented PET molecules have no lateral crystalline order. The results confirm that the nematic PET is grown to a smectic order.

The intensity of 001' reflection changes in the temperature range of 50–80°C depending on T_a and t_a. For temperatures T_a > 80°C, the intensity of 001' reflection clearly decreases, and at the same time, the triclinic 010 and $0\bar{1}1$ reflections appear as shown in Fig.4.1 d–f. The results indicate that the cold drawn PET is crystallized into the triclinic structure through the nematic to smectic states.

4.3.2 Analysis of the tilted orientation

At higher temperature above 100°C, the triclinic fiber pattern indicates the tilted orientation [6]. For precise analysis of the triclinic reflections, we used a cylindrical camera [1]. The WAXS of the cold drawn PET annealed at 150°C, 200°C and 250°C, are shown in Fig.4.2. Due to the tilted orientation, the reflections are displaced from the layer lines as mentioned in the introduction (4.1, pp31). By precise observation of the cylindrical patterns, amount of the displacement is found to be changed by T_a, demonstrating that the crystalline tilt varies with the annealing temperature. This fact is conflicted with the findings of the others [6,7], because the so-called ($\bar{2}30$) tilting must give the same displacement at any T_a.

The amount of displacement from the layer line is precisely measured from the WAXS patterns. Then the result is compared with the calculated value by changing the tilted direction and angle. The features of the fitting are illustrated in Fig.4.3, where the displacement in Fig.4.2 is well explained by the calculated positions.

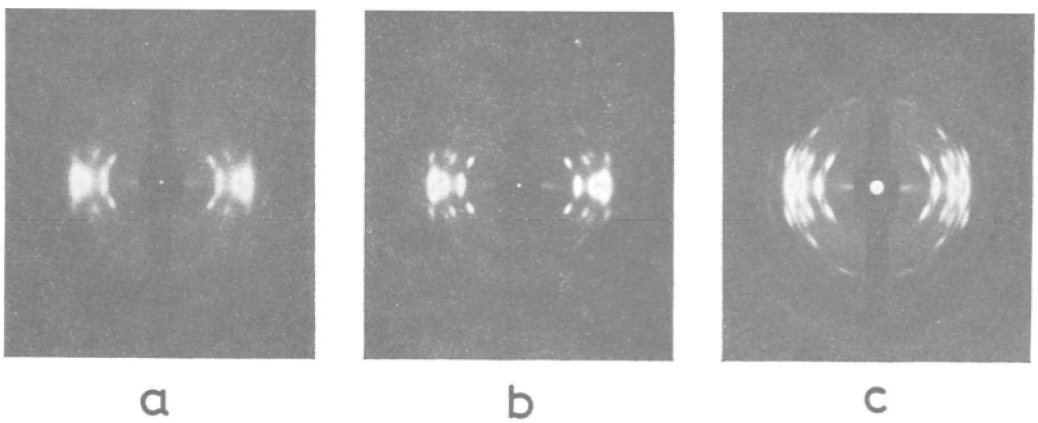

Fig. 4. 2 WAXS patterns of cold drawn PET by a cylindrical camera.
Annealing temperatures: (a) 150°C, (b) 200°C and (c) 250°C [1].

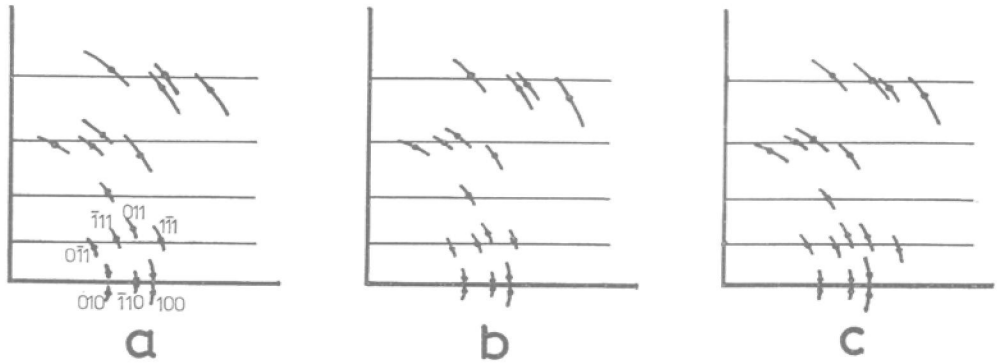

Fig. 4. 3 Displacement of the reflections from the layer lines: The arcs of (a), (b) and (c) correspond to the reflections of Fig.4.2 and dots show the calculated positions.[1]

By the analysis of the tilted orientation of the cold drawn PET, we have conclusions:

1. At low temperatures (100°C -150°C), the crystalline c-axis is tilted in the bc-plane by 5~8°. At high temperatures (200°C -250°C), the tilt direction is changed towards ac-plane where the tilt angle remains by 5°.
2. At low temperatures, the 010 and $0\bar{1}1$ reflections become sharper than other reflections. This fact indicates that the initial crystallization preferentially develops along the b-axis. At high temperatures, the triclinic crystal grows along a and b directions without the preference.
3. Accompanied with the preferential crystallization along the b-axis, the crystalline c-axis is tilted in the bc-plane at low temperatures. The observed variation of the tilted orientation is well explained by the preferential growth of the cold drawn PET.

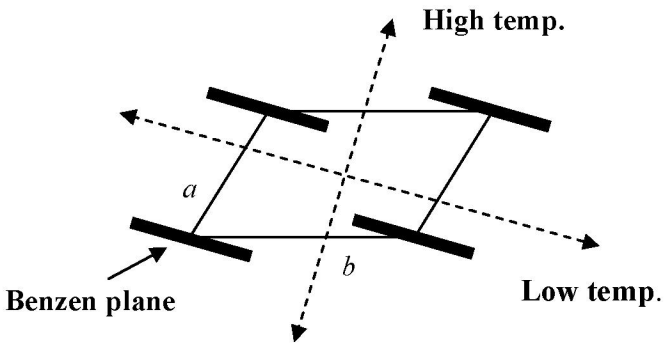

Fig.4.4 Projection of the triclinic crystal along the c-axis.
The dotted lines indicate the growth directions.

4. Considering the crystalline structure, PET has a benzene ring in the monomer unit. In the triclinic crystal, the benzene plane is inclined from the bc-plane by 15°. In the flat-sectioned polymers, the initial crystallization is preferentially developed along the flat plane. ***At low temperatures, the crystal is grown nearly parallel to the benzene plane as illustrated by the dotted line in Fig.4.4. On the other hand, at high temperatures, the crystal develops both parallel and perpendicular to the benzene plane. The tilted orientation is closely related to the crystalline growth direction.***

4.4 *In situ* Observation by MAXS

In order to analyze the initial crystallization, the cold drawn PET was fixed on the heating apparatus. During heating, the *in-situ* crystallization was measured by the synchrotron facility [2]. The results of the MAXS measurements are shown in Fig. 4.5 in which the isotropic rings are artifacts originated from the polymer film placed in the vacuum path. The meridional 001' reflection is located outside the isotropic ring as indicated in Fig. 4.5c. The 001' reflection appears at T_a = 50°C and completely disappears at T_a =100°C. On the other hand, the SAXS reflection appears near the center of the pattern at temperatures 70°C and above (Figs. 4.5 c–f). In Figs.4.5 d-f, the SAXS pattern appeared on the ellipsoid. From the SAXS reflection, the lamellar spacing along the Z-axis, L_Z, is measured. The values of L_Z are almost constant over the range of temperatures shown in Fig.4.5 and equal to 110 Å. Hence, the initial lamellae along the drawing direction will comprise roughly 10 monomer units. ***As the annealing temperature increases, the meridional reflection progressively weakens while the SAXS reflection increases in intensity. The most important result is that the smectic structure and the development of the triclinic lamellae are strongly correlated in the initial crystallization.***

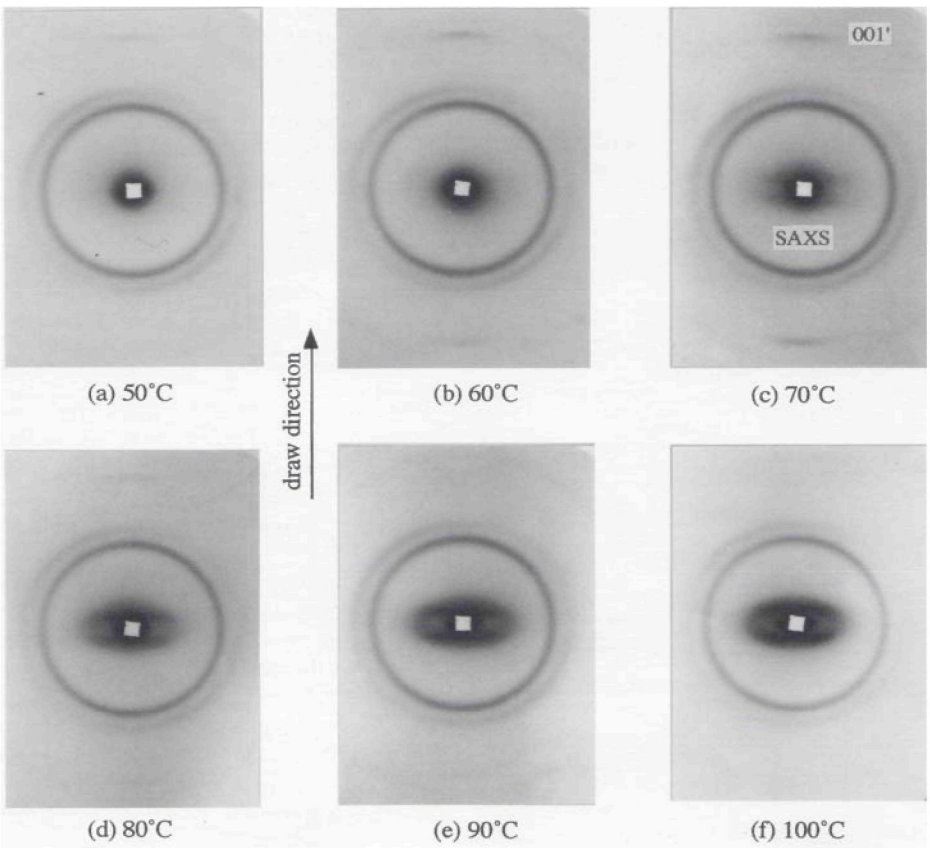

Fig. 4.5 In *situ* MAXS patterns of PET obtained at different annealing temperatures: (a) 50°C, (b) 60 °C, (c) 70 °C, (d) 80 °C (e) 90°C, (f) 100°C.
The MAXS patterns were observed during increasing T_a with the time interval of 30 sec in each pattern [2].

4.5 SAXS Measurements

4.5.1 4-Point SAXS pattern

SAXS measurements were performed on the cold drawn samples annealed at $T_a \geq$ 100 °C [8] for t_a=10^4 sec. As shown in Fig.4.6, the SAXS patterns reveal a typical 4-point pattern, where the intensity and shapes are changed by T_a. This difference is caused from the lamellar thickness as well as the lamellar inclination angle with respect to the draw direction. The increase of SAXS intensity with T_a is related to the internal structure of the lamellae. For the shape of the 4-point pattern, the streaks appear on the ellipsoid at T_a= 150°C, parallel to the equator at T_a= 200°C and on the hyperboloid at T_a= 240 °C. The relation between the SAXS pattern and the structure, together with the crystallization mechanism, is discussed in the following sections.

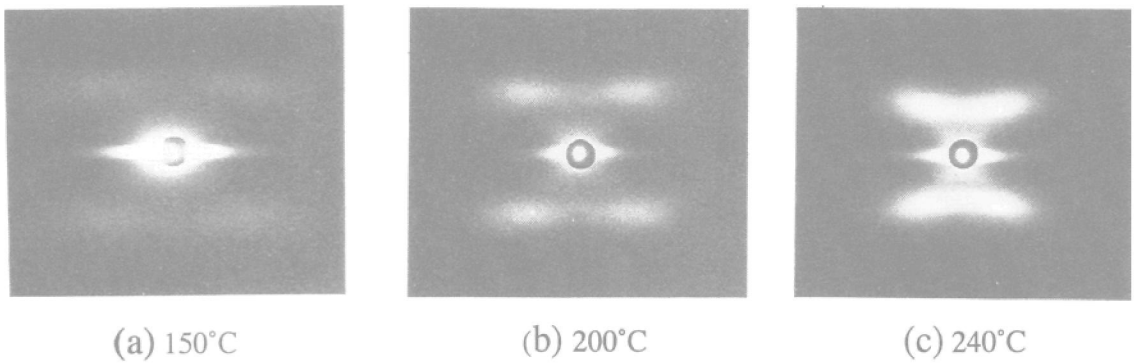

Fig. 4.6 SAXS patterns of drawn PET annealed at: (a) 150°C, (b) 200 °C, (c) 240 °C [12].

4.5.2 Evaluation of thickness and inclination of the lamellae

In order to analyze the 4-point pattern, we define here the lamellar spacing, L and the lamellar inclination angle ϕ, between the lamellar normal and the drawing direction.

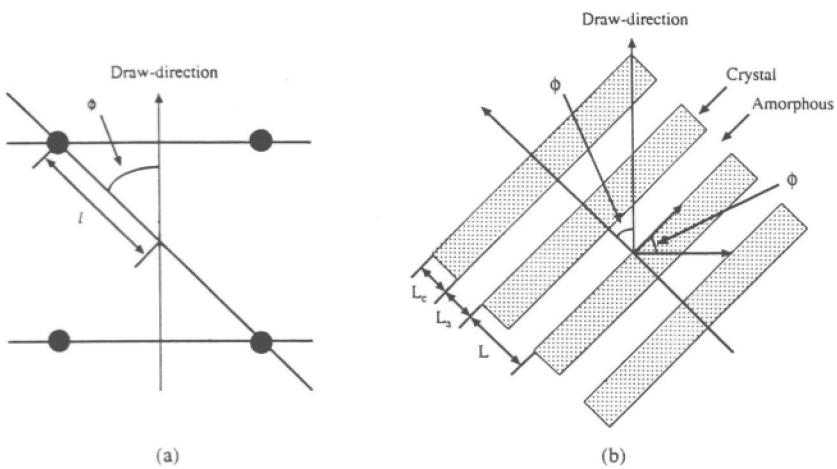

Fig. 4.7 Comparison of (a) the 4-point pattern and (b) the layer structure. The diagonal direction is parallel to the lamellar normal [12].

In the former section, we consider the lamellar spacing L_Z along the Z-axis. Then L_Z has a relation with L by the equation:

$$L=L_Z \cos\phi. \quad \text{(4.1)}$$

To determine L and ϕ, we draw a 4-point scheme as shown in Fig.4.7a. In the procedure of analysis, we at first fix the positions of 4-maxima where the diffraction intensity has a highest value. As indicated in Fig.4.7a, we measure the distance l, which is a half of the diagonal length of the 4-point, and angle ϕ.

The corresponding layer structure is illustrated in Fig.4.7b. The lamellar spacing, L is measured from the observed l. using Eqs.(1.3) and (4.1). For the SAXS measurement, it is possible to use the approximations: $\sin\theta \approx \theta$, and $\tan 2\theta \approx 2\theta$, when the value of θ is small. Then .

$$2\,L\sin\theta \approx 2L\theta = \lambda \quad \text{(4.2)}$$

$$\tan 2\theta \approx 2\theta = l/R, \quad \text{(4.3)}$$

where R is the camera length of the SAXS setting. As a result, L is calculated by:

$$L = R\lambda / l \quad \text{(4.4)}$$

The results of the observed values are listed in Table 4.1. Values of the lamellar spacing L increase whereas those of the inclination angle ϕ decrease with T_a.

Table 4.1. Long period in the drawing direction L_Z, lamellar inclination angle and lamellar spacing L of the cold drawn PET annealed at temperature T_a ($t_a = 10^4$ s) [2].

T_a (°C)	L_Z (Å)	ϕ (°)	L (Å)	α_c	L_c (Å)
100	110	60	55	0.22	14
120	111	56	62	0.28	20
140	113	52	70	0.35	28
160	117	49	77	0.41	35
180	120	47	82	0.48	44
200	124	45	88	0.55	52
220	140	41	106	0.63	70
240	158	37	126	0.72	91

4.5.3 Finer analysis of the layer structure

Following the two-phase model, polymer materials are consisted of crystalline and amorphous phases. Then, the volume degree of crystallinity, α_c, is derived from the sample density ρ by the following relation;

$$\alpha_c = (\rho-\rho_a)/(\rho_c-\rho_a), \quad \text{(4.5)}$$

where ρ_a and ρ_c are densities of amorphous and crystal phases, respectively.

According to Fig. 4.7b, the lamellar structure is composed of crystalline layers (L_c) and amorphous layers (L_a), where $L = L_c + L_a$. Using the value of α_c, we can calculate L_c by;

$$L_c = L\,\alpha_c. \quad \text{(4.6)}$$

The SAXS intensity is varied by the difference of electron densities between the

crystalline and amorphous layers. Normally, the intensity increases with L_c. However, the limit case when α_c =1, the SAXS diffraction will disappear. We discuss the relation of the SAXS intensity to the layer structure in the section 4.8 (pp44).

The shape change of the SAXS pattern with T_a can be understood by means of an angle, ε, which is defined as an angle between the diagonal and the normal to the streak as shown in Fig. 4.8. The variation of ε is possibly related to the lamellar fluctuation. The fine structures related to the SAXS intensity and the angle of ε related to the lamellar fluctuation will be discussed later with the help of a simulation technique using the light scattering (pp45).

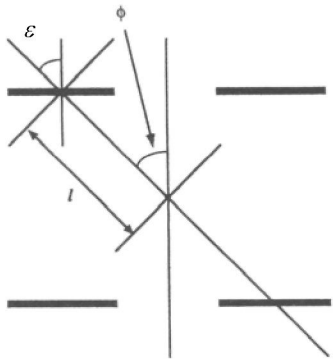

Fig. 4.8 Definition of the angle ε between the diagonal and the normal to the streak [12].

4.6 Crystallization Process of Cold Drawn PET

4.6.1 Initial crystallization at low temperatures

In order to summarize the various steps of the crystallization process, the results of the WAXS, MAXS and SAXS measurements are schematically illustrated in Fig. 4.9. MAXS results are summarized on the schemes of WAXS.

Starting from the glassy amorphous state, molecules are aligned to the draw direction showing the nematic order. By appearance of the 001' reflection, the nematic PET improves ordering to the smectic state. In the initial crystallization (80°C>T_a>100°C), the development of the triclinic lamellae is accompanied by the disappearance of the smectic reflection. Due to the preferential growth of the triclinic crystal along the b-axis, the c-axis shows the specific tilted-orientation.

4.6.2 Molecular orientation by cold drawing

The density of the drawn glassy PET sample measured at 20°C is 1.37g/cm^3. This value is higher than that of amorphous PET (1.335g/cm^3). The density monotonously increases with T_a. Some molecular segments could be randomly oriented or partly entangled owing to the limited mobility at temperatures well below T_g. However, considering the applied draw ratio of 3.8 and the increased density (1.37g/cm^3), it is reasonable to consider that a significant number of molecules are aligned nearly parallel to the draw direction. The orientational order exhibited by the PET molecules can be described by nematic state as schematically depicted in Fig.4.10a, where the circles in the molecular chains represent benzene rings separated by 10.75Å intervals. The lateral position of each benzene ring deviates with respect to the neighboring molecules.

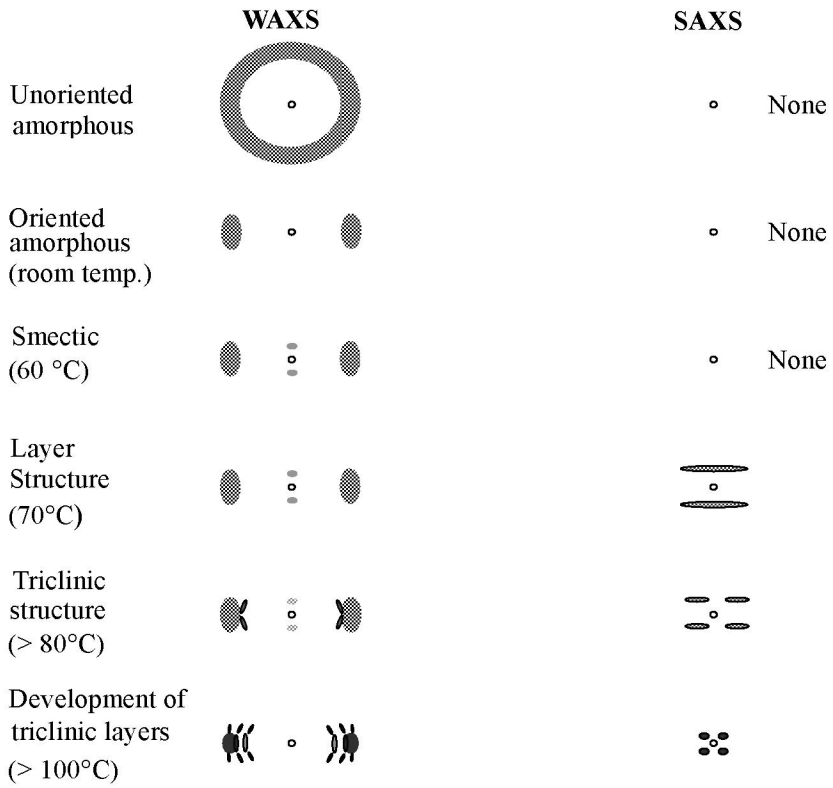

Fig. 4. 9. Summary of the X-ray results during the crystallization [2]

4.6.3 Analysis of the meridional reflection

The meriodional reflection is first apparent at temperatures below T_g. The spacing is almost equal to the monomer unit length, suggesting that neighboring molecular segments are laterally aligned with the benzene position. ***To explain this result, we consider the smectic order developed from the nematic state as shown in Fig. 4.10b. The benzene rings of the smectic state are arranged on planes perpendicular to the draw direction, whereas the lateral packing of the neighboring molecules has no crystalline order.*** The smectic state is presumably attained by increasing mobility of segments leading to the slightly higher densely (ρ=1.38g/cm^3) than that of the nematic phase.

4.6.4 Development of lamellar structure

A diffuse SAXS reflection appears at T_a=70°C (Fig.4.5c, pp35) prior to the development of the triclinic crystal. The result suggests the existence of a precursor state before the triclinic state. If we consider that T_a is the vicinity of T_g, molecular motions are not sufficient so as to form a layer structure giving the SAXS reflection. ***Hence, we propose a molecular tilting mechanism in the smectic phase which implies a minimum cooperative displacement. This tilting mechanism could produce a density difference within the smectic structure and hence could explain the structure observed by SAXS. As a result of the molecular tilting in the smectic state, the phase separation into triclinic crystalline and amorphous layers occurs at 80-100°C (Fig.4.10c).*** The precursor stage at T_a=70°C is schematically illustrated in Fig.4.11.

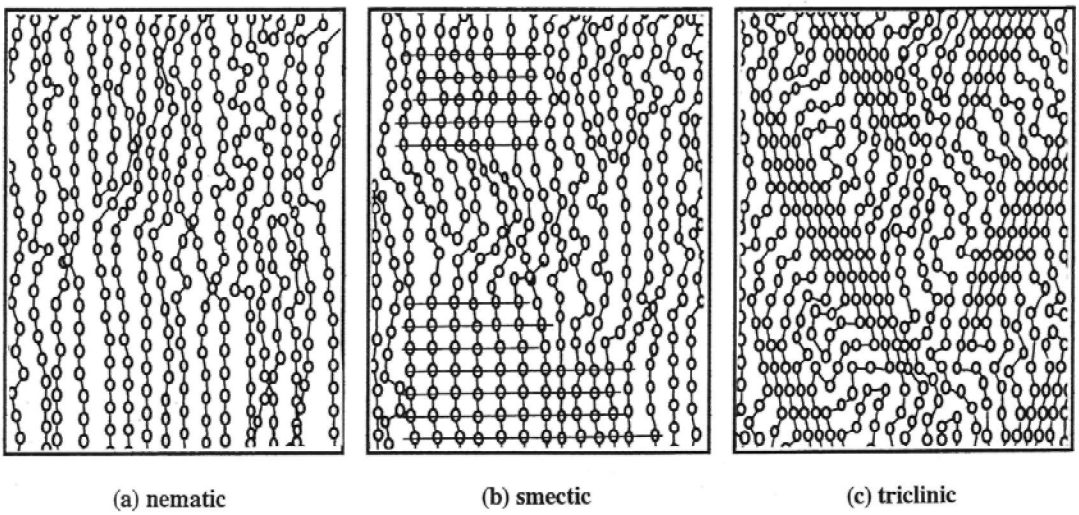

Fig. 4. 10 Schematic representation of the morphlogical changes: (a) nematic phase (b) smectic phase and (c) triclinic structure [2].

4.6.5 Tilting mechanism

One possibility to explain the periodic density difference observed along the molecular direction at T_a=70°C could be due to a combination of a molecular tilt mechanism and the inclination of the layer surface. To estimate the density difference along the molecular direction, we first calculate the average lateral distance between molecules in the smectic state. The volume of the triclinic unit cell, V_c, is 218.95 Å^3 [4]. The average smectic volume, V_{sm}, is estimated as follows:

$$V_{sm} = \frac{\rho_c}{\rho_{sm}} \times V_c = 230.85 \text{ Å}^3 \quad \ldots\ldots\ldots\ldots\ldots\ldots\ldots\ldots\ldots \quad (4.7)$$

where, ρ_c = 1.455 g/cm^3 [6], and ρ_{sm} = 1.38 g/cm^3 as a smectic density observed at 70°C. The average molecular cross section is derived as 230.85 Å^3/10.75 Å = 21.47 Å^2 and the average molecular distance is calculated as 5.23 Å. If we assume that the lamellar surface fits to the shift of one monomer unit (see Fig.4.11a), then the inclination angle ϕ of the lamella is calculated as:

$$\phi = \tan^{-1}\left(\frac{10.75}{5.23}\right) = 64° \quad \ldots\ldots\ldots\ldots\ldots\ldots\ldots\ldots\ldots\ldots\ldots \quad (4.8)$$

This value is consistent with the value (~ 62°) obtained from the MAXS pattern at 70°C (Fig.4.5c).

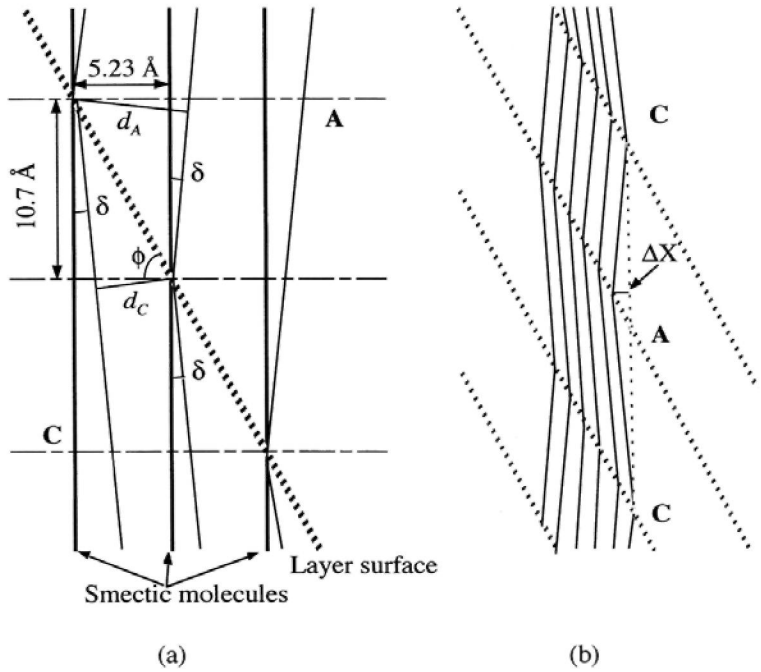

Fig. 4. 11 The tilting mechanism occurring in the precursor state: (a) The density difference between A and C regions, (b) The phase separation induced by the tilting by δ [2].

Assuming that the smectic molecules are tilted alternately by an angle $\pm\delta$ from the draw direction, the inclined layer produces packing difference between regions A and C (Fig.4.11a). The ratio between the densities in the A and C regions can be calculated from the ratio between the lateral dimensions in A and C, d_A/d_C. If we calculate the case of δ=1°:

$$\frac{d_A}{d_C} = \frac{\sin(90° - 64° + \delta)}{\sin(90° - 64° - \delta)} = 1.074 \quad \text{.....(4.9)}$$

On the other hand, the quotient between the amorphous and the triclinic density is equal to:

$$\frac{\rho_c}{\rho_a} = \frac{1.455}{1.370} = 1.062 \quad \text{.....(4.10)}$$

Thus, the estimated d_A/d_C ratio in the precursor state seems to be sufficient to produce the required density contrast. Moreover, using δ=1° and L= 110 Å, the lateral deviation from the draw direction, Δx, is less than 1 Å (Fig.4.11b). The small δ and Δx values are possible to occur in the initial stages of crystallization at T_g. The aforementioned discussion strongly suggests that a tilting mechanism could produce the precursor state at 70 °C.

4.6.6 Development of triclinic crystals

The results of WAXS (Fig.4.1) indicate that the triclinic crystal develops above 80 °C. In the preceding section, we suggest that the precursor state is formed by a slight tilt of the smectic molecules. The triclinic structure is then developed at T_a> 80 °C by a further tilt of the molecules within the crystalline lamellae. In Fig.4.1f, the triclinic (010) plane is inclined

by 8~10° from the draw direction. Considering the triclinic structure [6] with crystallographic angle α = 98.5°, the crystalline b-axis is nearly perpendicular to the draw direction. This fact supports that the triclinic (001) plane is perpendicular to the draw direction. Figure4.10c schematically shows the development of the triclinic crystals at 100 °C. Further annealing at high temperatures will thicken the crystalline lamellae as shown in Table 4.1.

In the initial crystallization of cold drawn PET, mechanism from the smectic, via the precursor, into the final triclinic state is explained by the tilting mechanism. The slight tilt in the inclined layer surface effectively produces a density difference between crystalline and amorphous regions in the precursor state.

4.7 Effect of the Drawing Temperature

In the above discussions, we have studied the case of the cold drawn PET. We compare here the case of the hot drawn sample. The glassy amorphous PET was drawn at 90°C with drawing speed of 30 mm/sec. Then the sample was annealed without shrinkage at 150°C for 10^4 sec. The WAXS pattern shows that the crystalline c-axis is largely inclined (about 30°) from the draw direction (Fig.4.12c). The SAXS pattern displays a typical 2-point pattern (Fig.4.12d). As observed in the cold drawn PET (Figs. 4.12a and b), molecules are highly oriented, whereas the lamellae are inclined from the draw-direction. ***In the hot drawn PET, molecules are highly inclined, while the lamellar normal becomes parallel to the draw-direction. The results are schematically displayed in Fig. 4.13. The supplementary effect appears in the molecular and lamellar inclinations in the both cases.***

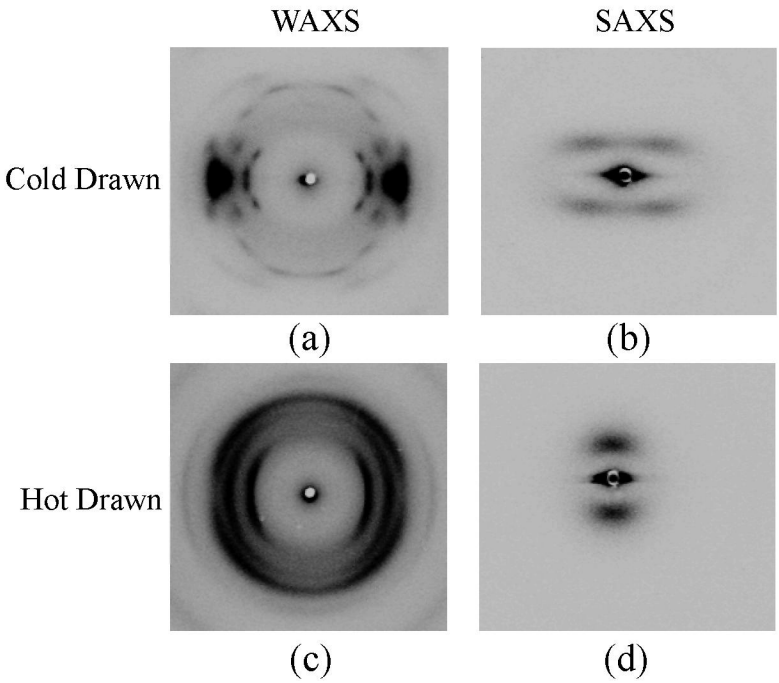

Fig.4.12 Comparison of the cold- and hot-drawn PET

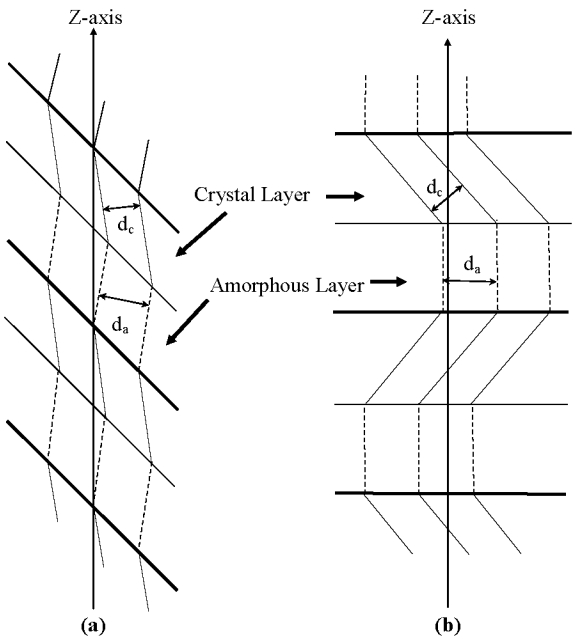

Fig. 4.13 Comparison of the lamellar structures annealed at 150 °C:
(a) In the cold drawn PET, molecules are nearly parallel to the Z-axis and layers are largely inclined shown by the 4-point SAXS pattern.
(b) In the hot-drawn PET, layer is flat indicated by the 2-point pattern where the crystalline molecules are largely inclined from the Z-axis.
The dotted lines in the amorphous layer demonstrate the average molecular direction. The disordered segments including chain folding are concentrated in the amorphous layer.

4.8 Simulation by Light Scattering

4.8.1 Analysis of the smectic structure

To examine the relation between the width of smectic region (real space) and the sharpness of the reflection (reciprocal space), we define w and d_s as the width of smectic region and layer spacing, respectively. For the simulation, smectic layers are depicted by thick black lines, aligned perpendicular to the meridian separated by d_s. In Fig. 4.14, the scattering patterns are measured by changing w/d_s ratio from 0.5 to 6.0. ***The results indicate that the meridional reflection becomes sharp with increasing the ratio, and a point-like reflection appears when $w/d_s > 4$.*** From these findings, the width of the smectic region can be estimated larger than $w/d_s \approx 4$. If we consider the average smectic spacing being $d_s \approx 10$ Å, the sharp 001' reflection, observed in Figs. 4.1 and 4.5, will appear when $w \approx 40$ Å. Assuming an average molecular distance ≈ 5 Å, the possible smectic region with the cross-section $(40\ \text{Å})^2$ consists of $(40/5)^2 = 64$ molecules.

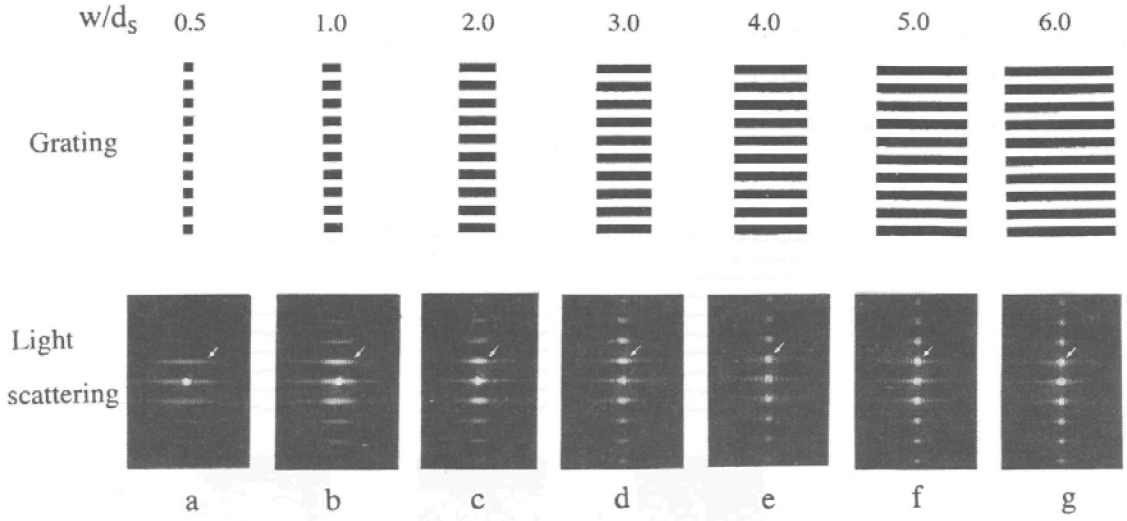

Fig. 4.14 Simulation of light scattering to observe the effect of the smectic width on the sharpness of the meridional reflection [12].

4.8.2 Analysis of the SAXS intensity

In the layer structure, we consider $L = L_c + L_a$. The relation of SAXS intensity with L_c (crystalline layer) is simulated in Fig.4.15. Here, L_c is represented by the black lines of the grating. The ratio L_c/L is changed by 10-90%. The result is given under each ratio, showing a change of intensity (arrows from a to e). ***While the minimum intensity appears at L_c/L= 10 and 90%, the maximum intensity is attained at L_c/L = 50%.*** These facts indicate that an increase of L_c makes an increase in SAXS intensity until the ratio becomes 50%. In Table 4.1, the crystallinity is 0.55 and 0.72 at T_a=200°C and 240°C, respectively. However, the SAXS intensity is higher at T_a=240°C. This fact suggests that the surface of the crystalline layer includes some imperfect region.

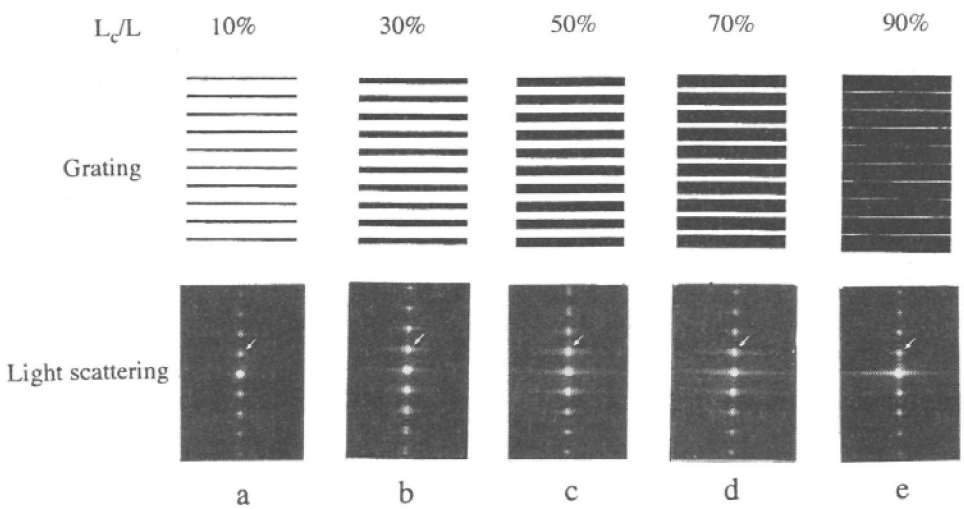

Fig. 4.15 Simulation of the thickness of crystalline lamellae [12].

4.8.3 Analysis of the SAXS streak

The shape change of the SAXS reflection is examined by the light scattering. In Fig.4.16b, the layer structure has a fluctuation perpendicular to the layer plane. The corresponding light scattering has a streak perpendicular to the fluctuation. In Fig.4.16a and c, the fluctuation is displaced in the opposite direction from Fig.4.16b. The displacement angles are adjusted to $\varepsilon = -20°$, 0° and 20° in Fig. 4.16a and c, respectively. Thus, the resulting diffraction patterns exhibit that the streak is inclined by -20°, 0° and 20° from the meridian.

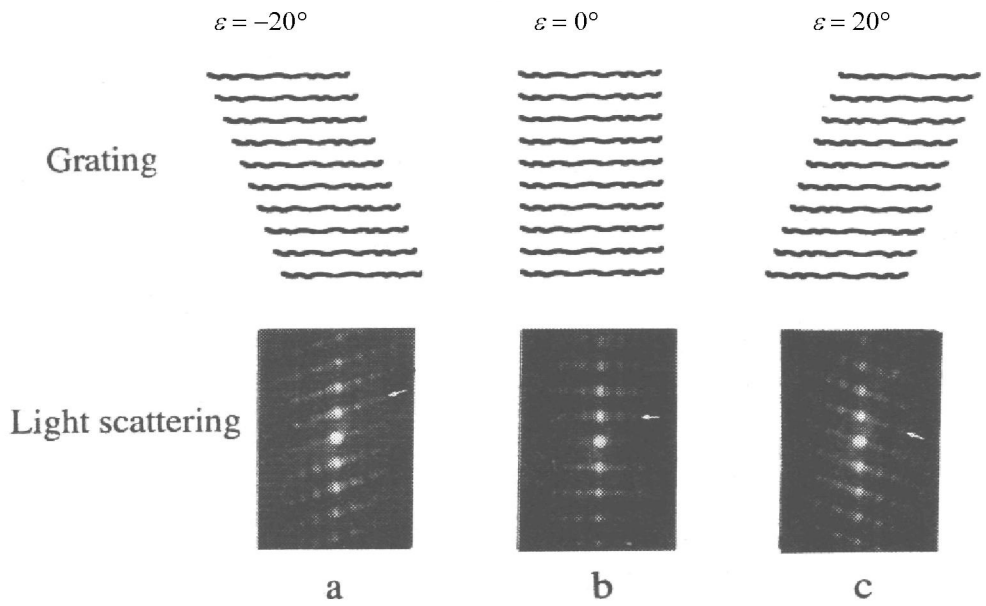

Fig. 4.16 Simulation of the effect of lamellar fluctuation [12].

4.8.4 Analysis of the 4-point pattern

The results of light scattering strongly indicate that the streak in the reflection appears from the displacement of the layer fluctuation. The direction of the streak is perpendicular to the displacement. Thus the results of the light scattering can be extensively applied to the fine analysis of the 4-point pattern. The SAXS patterns of Fig. 4.6 are analyzed by means of ϕ and ε. Here, we consider the inclined and displaced lamellar structure with respect to the draw-direction. The observed values are listed in Table 4.2, where ϕ decreases and ε increases with T_a. The results obtained are illustrated in Fig.4.17. Using another pair of the reflections in the 4-point pattern, the symmetrical layer structure by rotation around the draw direction is also possible to exist. In the real space pictures, the direction of the displacement is calculated by the angle $\varepsilon-\phi$. The displacement may be related to the macroscopic fibril direction, along where the molecular chains are averagely running.

Table 4.2. Layer structure of cold-drawn PET.

T_a (°C)	L_Z (Å)	ϕ (°)	L (Å)	ε (°)	$\varepsilon-\phi$ (°)	α	L_c (Å)
150	115	50	74	35	-15	0.40	30
200	124	45	88	45	0	0.55	48
240	158	37	126	55	18	0.75	95

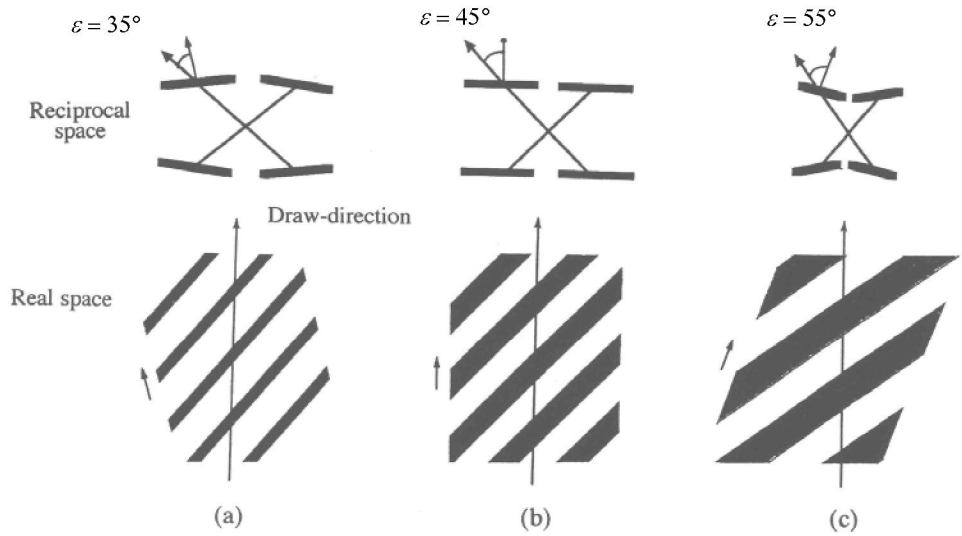

Fig. 4. 17 Analysis of the SAXS pattern corresponding to Fig.4.6, annealed at (a)150, (b) 200, and (c) 240°C [12].

The inclined and displaced lamellae are illustrated in the real space. The inclined black lines indicate the crystalline lamellae with interval of the amorphous layers. The distorted rectangle shows the direction of the displacement (corresponding to a fibril development).
The symmetrical structures around the draw direction are possible to exist.

4.9 Concluding Remarks

The crystallization of cold drawn PET has been studied by X-ray diffraction. ***Starting from the nematic state, the initial crystallization grows through the smectic structure***. The SAXS maxima observed at 70 °C indicates ***a precursor stage*** before the triclinic crystallization. At 80 °C, the triclinic crystal develops along the b-axis, where the (010) planes are inclined by 8-10° from the draw direction. ***The crystallization mechanism from the smectic structure, via precursor state, into the final triclinic crystal is explained by the tilting mechanism.*** The molecular tilt and the inclination of the lamellar surface produce a density difference between the amorphous and crystalline regions. ***The triclinic lamellae are developed accompanying the tilted orientation.*** The sharpness of the smectic reflection, the change of SAXS intensity and the shape change of the SAXS streak are well explained based on the simulation by the light scattering.

References

1. T. Asano and T. Seto, *Polym. J.*, **5**, 72 (1973).
2. T. Asano, F. J. Baltá Calleja, A. Flores, M. Tanigaki, M. F. Mina, C. Sawatari, H. Itagaki, H. Takahashi, I. Hatta, *Polymer*, **40**, 6475 (1999).
3. R. Bonart, Kolloid-*Z.*, **213**, 1 (1966).
4. G. S. Y. Yeh and P. H. Geil, *J. Macromol. Sci.*, **B1** 235 (1967)
5. G. S. Y. Yeh and P. H. Geil, *ibid.*, **B1** 251 (1967)
6. R. de P. Daubney, C. W. Bunn and C. J. Brown, Proc. Roy. Soc. (London), Ser A, **226**, 531 (1954).
7. R. Bonart, Kolloid-*Z.*, **199**, 136 (1964).
8. H. G. Zachmann, H. A. Stuart, *Macromol. Chem.*, **41**, 131 (1960)
9. G. Elsner, MHJ. Koch, J. Bordas, H. G. Zachmann, *Macromol. Chem.*, **181**, 1263 (1981)
10. G. Elsner, C. Riekel, H. G. Zachmann, *Adv. Polym. Sci.*, **67**, 1 (1985)
11. B. Günter, H. G. Zachmann, *Polymer*, **24**, 1008 (1983)
12. T. Asano, A. Saeki, M. F. Mina, M. Tanigaki, *Rep. Fac. Sci., Shizuoka Univ.*, **33**, 23 (1999).
13. T. Asano, A. Dzeick-Pickuth and H. G. Zachmann, *J. Mater. Sci.*, **24**, 1967 (1989).
14. A. Flores, F. J. Baltá Calleja and T. Asano, *J. Appl. Phys.*, **90**, 6006-6010, 2001.